Electronic supplementary materials *Mendeleev Commun.*, 2022, **32**, 123-125

Copper(II) perchlorate complexes with antipyrine: synthesis, structure, cytotoxicity and DFT calculations

Nataliya S. Rukk, Grigory A. Buzanov, Nikita S. Kabernik, Lyudmila G. Kuzmina, Galina A. Davydova, Nikolay N. Efimov, Ravshan S. Shamsiev, Svetlana K. Belus, Evgeniya I. Kozhukhova, Vasilii M. Retivov and Taisiya V. Ivanova

Copper(II) perchlorate was obtained by the reaction of basic copper(II) carbonate ($Cu(OH)_2 \cdot CuCO_3$) and perchloric acid, taken in a molar ratio Cu-containing compound**:** $HClO_4$ = 1:2. The resulting dark blue solution was heated until 60-70% water evaporated. The copper content in dark blue crystals obtained after cooling was determined by titrimetric analysis, and the compound composition $Cu(ClO_4)_2 \cdot 6H_2O$ was confirmed. Antipyrine was obtained from commercial sources and recrystallized from water or ethanol. Preliminary prepared $Cu(ClO_4)_2 \cdot 6H_2O$ (0.9263 g, 2.5 mmol)) was dissolved in a minimum volume of distilled water and mixed with an aqueous solution of the calculated antipyrine amount (0.9411 g, 5 mmol); 1.8823 g (10 mmol); 2.3528 g (12.5 mmol) or 2.8234g (15 mmol) for the Cu:AP molar ratios 1:2, 1:4, 1:5; 1:6, respectively.

Calc. (wt. %) for $C_{44}H_{50}Cl_2CuN_8O_{13}$ (**1**) (1033.36): Cu, 6.15; C, 51.14; N, 10.84; H, 4.88. Found (wt. %): Cu, 6.49; C, 51.42; N, 11.10; H, 5.02.

Calc. (wt. %) for $C_{55}H_{60}Cl_2CuN_{10}O_{13.25}$ (2) (1207.57): Cu, 5.26; C, 54.70; N, 11.59; H, 5.01. Found (wt. %): C, 54.46; N, 11.40; H, 5.15.

Calc. (wt. %) for $C_8H_{12}ClCuN_4O_4$ (**3**) (327.21): C, 29.37; N, 17.32; H, 3.70. Found (wt. %): C, 29.56; N, 17.32; H, 3.66.

IR-spectra (cm^{-1}): (IR–Fourier spectrometer EQUINOX 55, «BRUKER», Germany; 4000 – 400 cm^{-1} (KBr pellets) (**1**): 1101 $\nu_3(ClO_4)$; 1574 ν(Cu-O)+ν(C=O); 1602 $\delta(H_2O)$ (Table S1). (**2**): 1082 $\nu_3(ClO_4)$; 1566 ν(Cu-O)+ν(C=O); 1651 ν(C=O) (Table S1).

ESI-MS spectra (electrospray mass spectrometer AmaZon Bruker Daltonik GmbH, UltraScan positive and negative ionization mode; m/z range: 70–2200; saline solution; 240 μL h^{-1}; needle source voltage 3.5 kV, carrier gas flow rate 6 L min^{-1}; capillary temperature 100° C, signal accumulation 300000 ions in the ion trap, signal averaging of 14 scans; Figure **S1)**.

For $[Cu(AP)_4(H_2O)](ClO_4)_2$ (**1**) the signals in the positive mode (found./calcd.) at 189.102/189.102, 211.086/212.092, 269.042/270.050, 399.180/397.907, 521.117/521.075 are assigned to APH^+, $APNa^+$, $APNa_2Cl^+$, $(AP)Na_2Cu_2Cl^+$, $(AP)_2ClCuNa_2^+$ and in the negative mode at 198.902/198.801, 220.885/220.987, 232.758/232.762, 466.755/460.869, 588.692/585.994, 710.629/709.161, 832.565/834.327, 956.499/265 and 1078.437/1079.345 are assignined to $Cu_2Cl_2^-$, $Cu_2Cl_2Na^-$, $Cu_2Cl_3^-$ $(C_{11}H_{12}N_2O)Cu_4(H_2O)^+$, $(C_{11}H_{12}N_2O)_2Cu_3(H_2O)^+$, $(C_{11}H_{12}N_2O)_3Cu_2(H_2O)^+$, $(C_{11}H_{12}N_2O)_4Cu(H_2O)^+$, $(C_{11}H_{12}N_2O)_4Cu(H_2O)(ClO_4)Na^+$, $(C_{11}H_{12}N_2O)_4Cu(H_2O)(ClO_4)_2Na_2^+$ respectively (Figure **S1** a, b).

For $[Cu(AP)_5](ClO_4)_2$ (**2**) the signals in the positive mode (found./calcd.) at 189.03/189.23, 291.93/291.90, 386.99/386.23, 407.58(815,116)/408.23(816.45), 440.0/440.46, 493.63/493.13, 552.10/551.56 are assigned to APH^+, $NaCu_2Cl_4^+$, $[Cu_2(AP)Cl_2]$, $[Cu(AP)_4]^{2+}$, $[Cu(AP)_2]$, $[Cu_2(AP)Cl_4(H_2O)_2]$, $[Cu_2(AP)Cl_4(H_2O)_2(NaCl)]$, and in the negative mode at 262.45/262.44, 274.57/274.78, 288.61/287.23, 361.46/360.55, 386.99/386.23 are assigned to $Cu(ClO_4)_2$, [NaCuAP], $[Cu(AP)Cl]^-$, $[Cu_4Cl_3]^-$, $[Cu_2(AP)Cl_2]$, respectively (Figure **S1** c, d).

EPR spectra were recorded on a Bruker Elexsys E-680X spectrometer operating at 9.8 GHz (X-band, room temperature; modulation amplitude: 5 Gs; power of microwave radiation: 2 mW). Theoretical EPR spectra were constructed by using EasySpin computational package[29] (Figures **S2,S3**; here and further, the reference numbers stand for those in the main text).

Powder X-ray diffraction patterns of the bulk samples (Bruker D8 Advance diffractometer of the Centre of Shared Equipment of IGIC RAS, CuKα radiation, Ni-filter, LYNXEYE detector, reflection geometry; 2θ range: 5º – 80º; step: 0.01125º) exhibit a good agreement with those calculated from the single crystal measurements (Figures **S4**,**S5**).

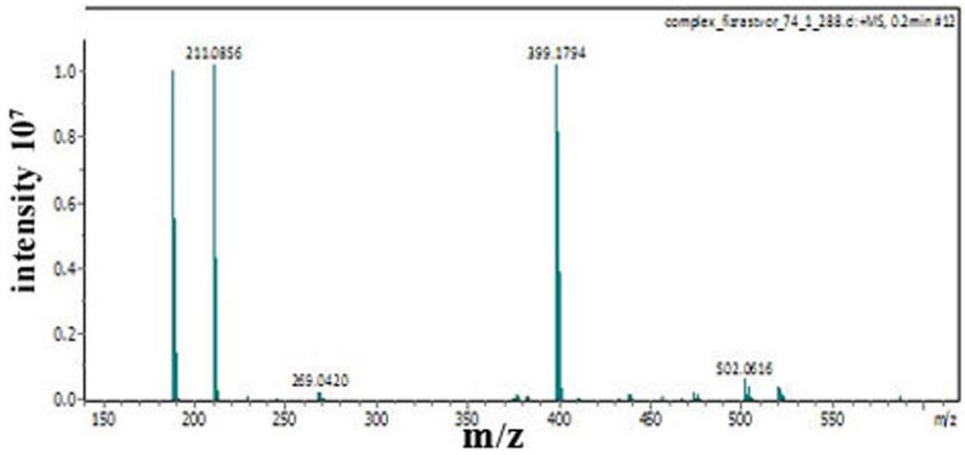

a

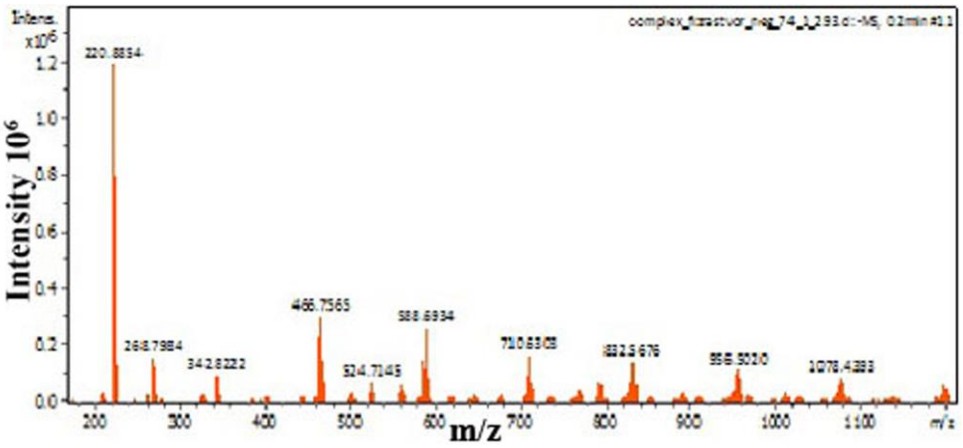

b

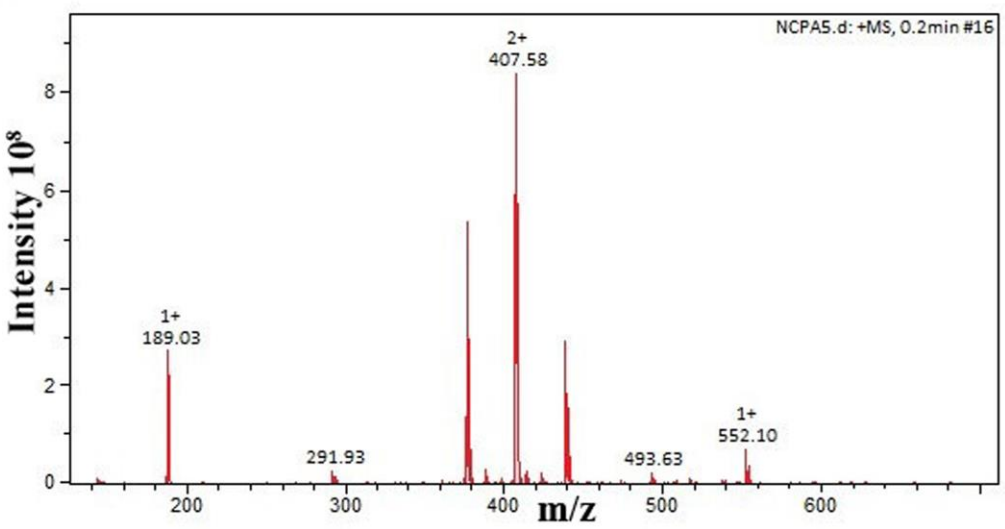

c

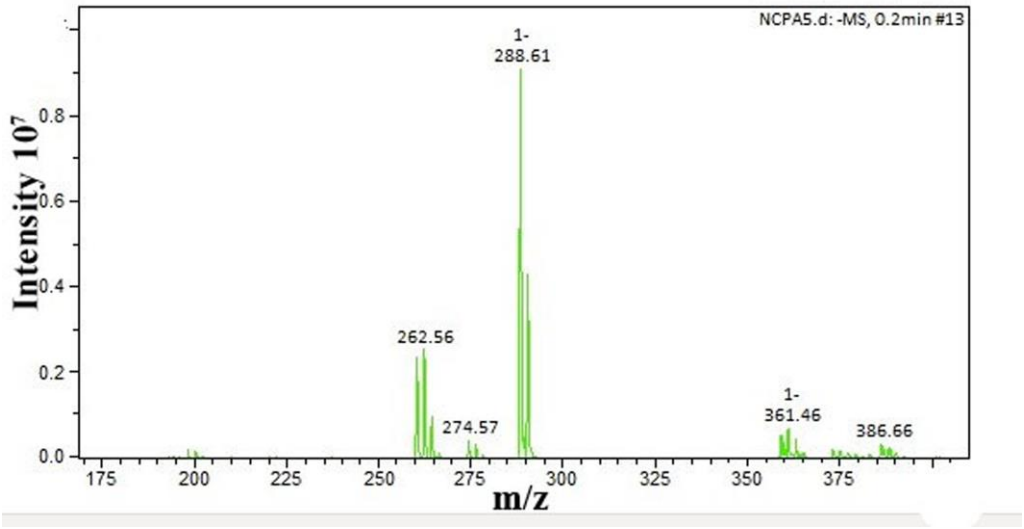

d

Figure S1 ESI-MS spectra of $[Cu(C_{11}H_{12}N_2O)_4(H_2O)](ClO_4)_2$ (**1**) (positive (a) and negative mode (*b*)) and $[Cu(C_{11}H_{12}N_2O)_5](ClO_4)_2$ (**2**) (positive (*c*) and negative mode (*d*))

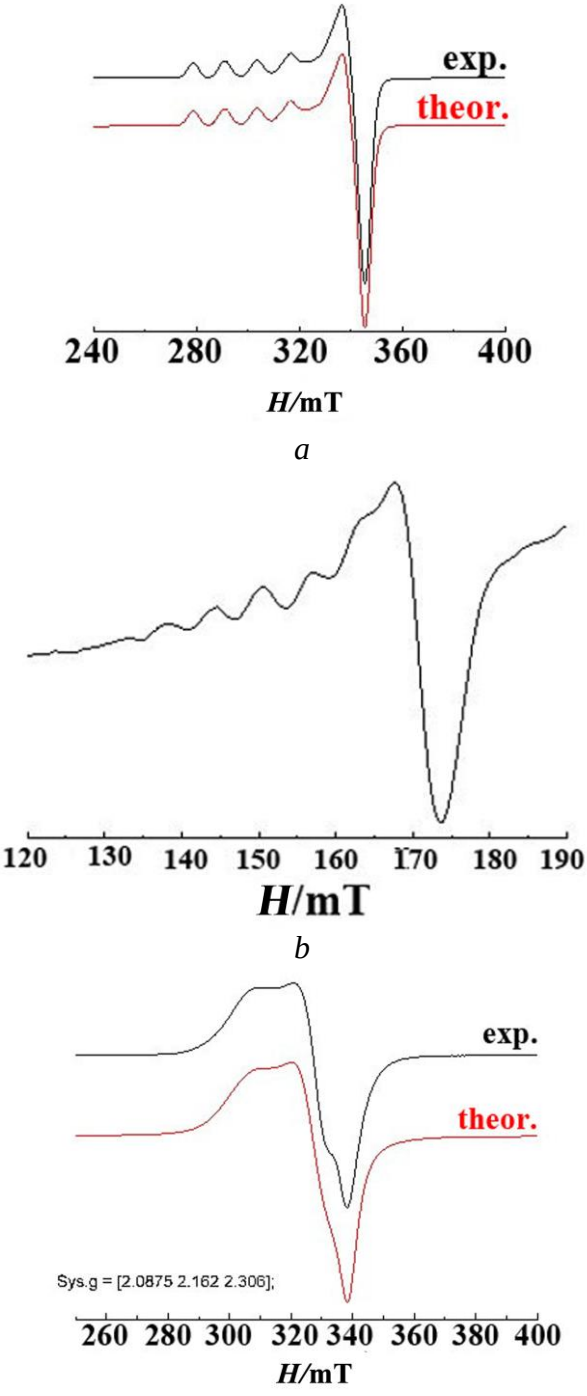

Figure S2 Experimental (exp.) and theoretical (theor.) EPR spectra for polycrystalline powder sample of $[Cu(C_{11}H_{12}N_2O)_4(H_2O)](ClO_4)_2$ (**1**) *a*); "Forbidden" transition in the EPR spectrum of $[Cu(C_{11}H_{12}N_2O)_4(H_2O)](ClO_4)_2$ (**1**) polycrystalline powder (293 K, X-band) in the "half" field (81 accumulations) *b*); Experimental (exp.) and theoretical (theor.) EPR spectra for polycrystalline powder sample of $[Cu(C_{11}H_{12}N_2O)_5](ClO_4)_2$ (**2**) *c*); (293 K, X-band).

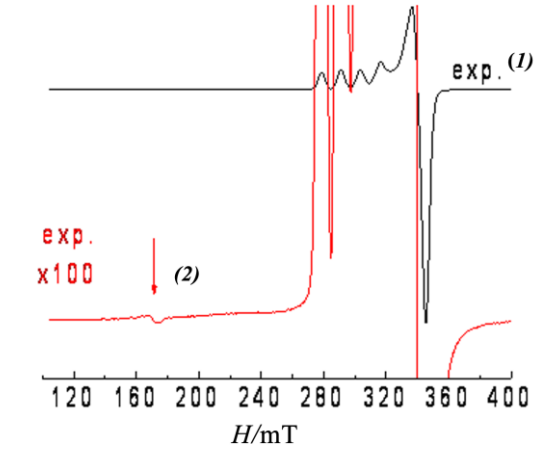

a)

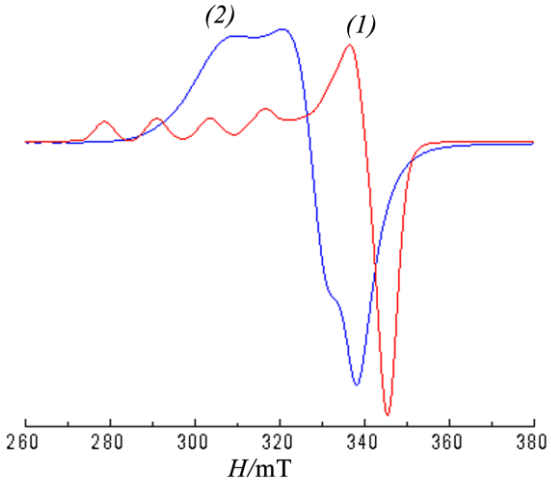

b)

Figure S3 The ratio of intensities of the allowed transition for the mononuclear complex $[Cu(C_{11}H_{12}N_2O)_4(H_2O)](ClO_4)_2$ (**1**) (black line, ***(1)***) and the "forbidden" transition indicating the presence of binuclear fragments with S = 1 (red line, ***(2)***). The relative magnification in the spectrum is 100 times a); Comparison of ESR spectra for polycrystalline powder samples of (**1**) (red line, ***(1)***) and (**2**) - blue line, ***(2))*** b)..

The EPR spectrum of (**1**) is described by the spin Hamiltonian for the monomer with hyperfine interaction:

$$\hat{H} = g_z\beta H_z\hat{S}_z + g_x\beta H_x\hat{S}_x + g_y\beta H_y\hat{S}_y + A\hat{I}_z\hat{S}_z,$$

where g_z, g_x, g_y are the x-, y-, and z-components of the g-tensor, A is the z-component of the HFS tensor; $\hat{S}_z$, $\hat{S}_x$, $\hat{S}_y$ are the projections of the spin operator on coordinate axes (S = 1/2), $\hat{I}_z$ is the projection of the nuclear spin operator of the central atom on the z-axis (I = 3/2). The best-fit of the experimental spectrum to the theoretical one (Figure S2, *a*) was achieved at the

following values of the spin Hamiltonian parameters: g_x= 2.053, g_y= 2.080, g_z= 2.373; A = 0.0135 cm^{-1} (404.7 MHz). The results obtained are in good agreement with the literature data ((g_x= 2.0686, g_y= 2.0957, g_z= 2.4311; A_z = 0.013 cm^{-1})[24], (g_x= 2.0376, g_y= 2.0360, g_z= 2.3416; A_z = 0.3651, A_x = 0.0870, A_y = 0.0473 GHz, 295 K)[25] for similar compounds and indicate that the system is anisotropic with tendency towards axial symmetry. It should be underlined that in a "half" magnetic field a low-intensity "forbidden" transition is observed (g ~ 4). As a result of 81 accumulations it was possible to obtain the spectrum of the "forbidden" transition with a good signal-to-noise ratio (Figure S2, *b*). The "forbidden": transition presence points to the fact that in the system under studies there is a state with the total spin of S = 1 which is specific to copper binuclear complexes[30]. In this case at the "forbidden" transition the HFS from the interaction with the nuclei of two copper ions is observable. It should be taken into account that the sensitivity of the EPR method in general and the equipment applied in particular is extremely high and the integral intensity of the forbidden transition shown in Figure **S2 b** is small (see Figure **S3 a**). The data obtained make it possible to confidently confirm that the concentration of binuclear fragments in the sample under study did not exceed 0.1%. For the parallel orientation of the g-tensor one can see four equidistant hyperfine structure (HFS) lines (Figure **S2 b**) from interaction with copper nucleus (I_{Cu}= 3/2).

The EPR spectrum of (**2**) is described by the spin Hamiltonian with the g-tensor three-axis anisotropy:

$$\hat{H} = g_z\beta H_z\hat{S}_z + g_x\beta H_x\hat{S}_x + g_y\beta H_y\hat{S}_y,$$

where g_z, g_x, g_y are the x-, y-, and z-components of the g-tensor, $\hat{S}_z$, $\hat{S}_x$, $\hat{S}_y$ are the projections of the spin operator on coordinate axes (S = 1/2). The best-fit of the experimental spectrum to the theoretical one (Figure **S2c, S3b**) was achieved at the following values of the spin Hamiltonian parameters:

g_x= 2.088, g_y= 2.162, g_z= 2.306 and slightly deviate from those ((g_x= 2.0376, g_y= 2.0360, g_z= 2.3416; A_z = 0.3651, A_x = 0.0870, A_y = 0.0473 GHz, 295 K) given in the article[25].

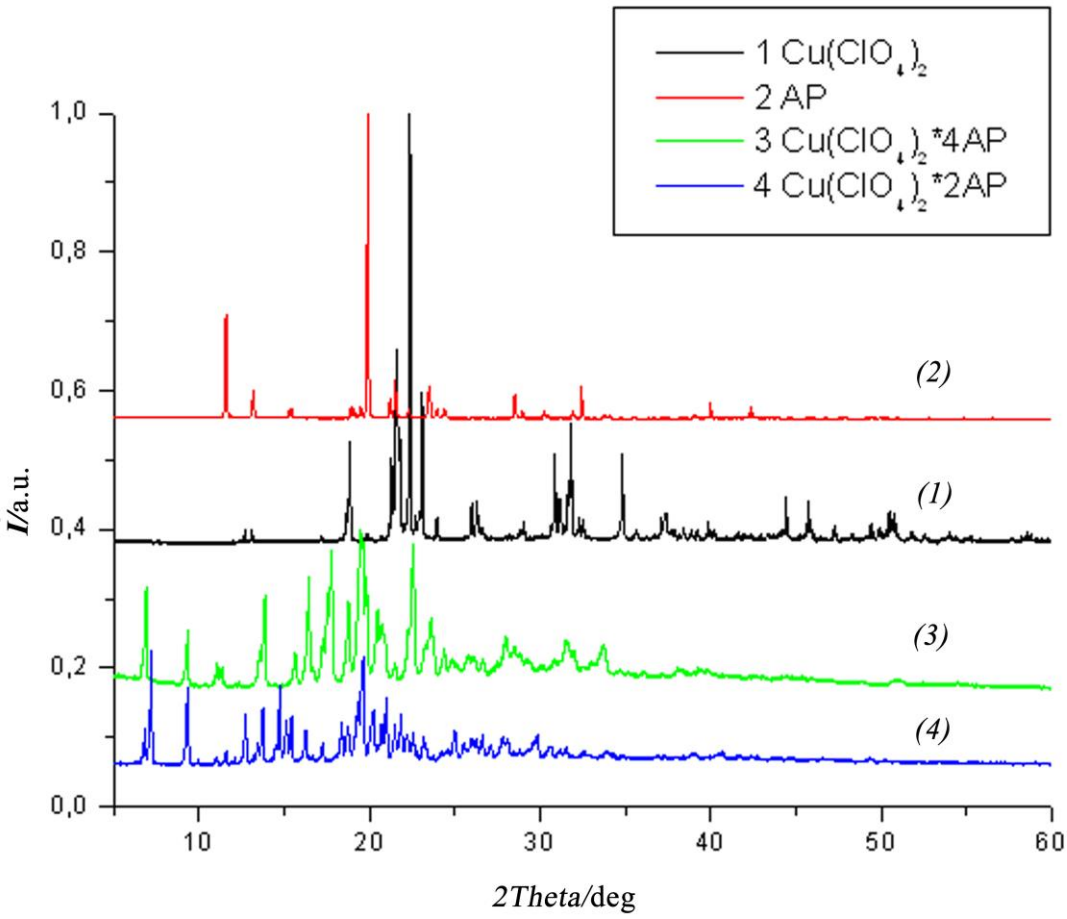

Figure S4 Diffraction patterns of the starting materials: $Cu(ClO_4)_2$; AP, and the complex with different amounts of ligand: $Cu(ClO_4)_2 \cdot 2AP$; $Cu(ClO_4)_2 \cdot 4AP$

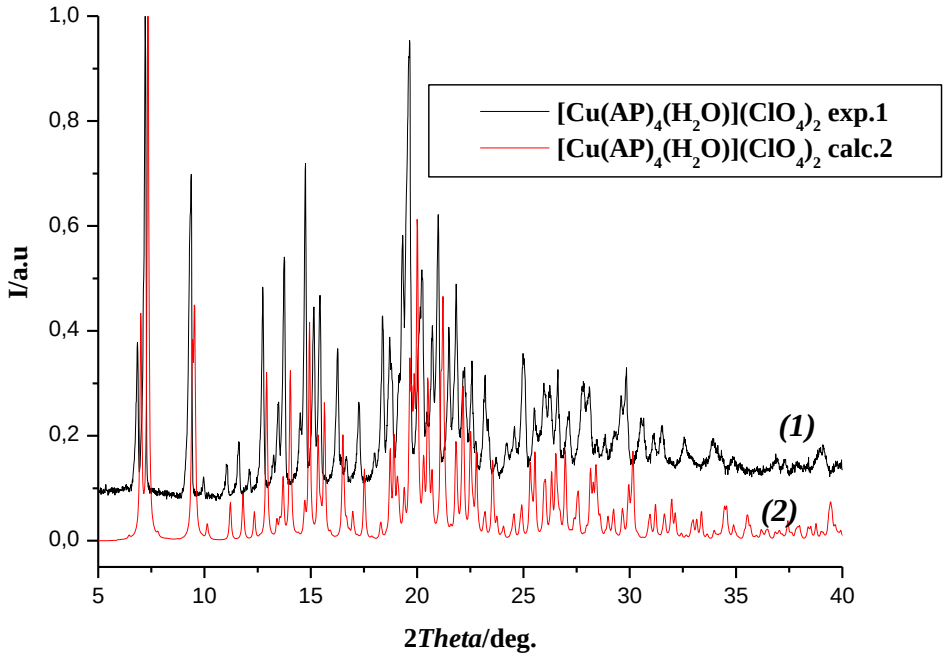

a)

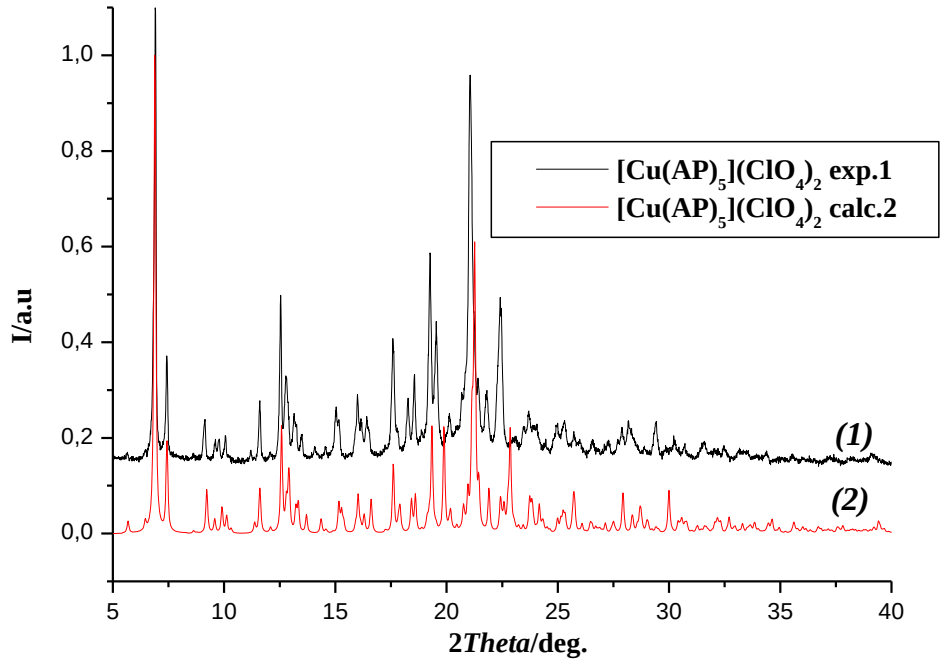

b)

Figure S5. Comparison of theoretical and experimental pXRD patterns:
a) $[Cu(AP)_4(H_2O)](ClO_4)_2$. *b*) $[Cu(AP)_5](ClO_4)_2$

[**]MTT test was also used for evaluation of the (**1**) and (**2**) influence on the proliferative activity of 10 different cancer cell lines: C6 rat glioma, Panc-1 human pancreatic carcinoma. U-251 human glioma, IMR32 human neuroblastoma, HS 578-T and BT474 human breast cancer, HEK293 human embryonic kidney, Hep-2 Human Epithelioma-2, MNNG-HOS human osteosarcoma and SH-SY5Y human neuroblastoma-like cells (Figure S6).

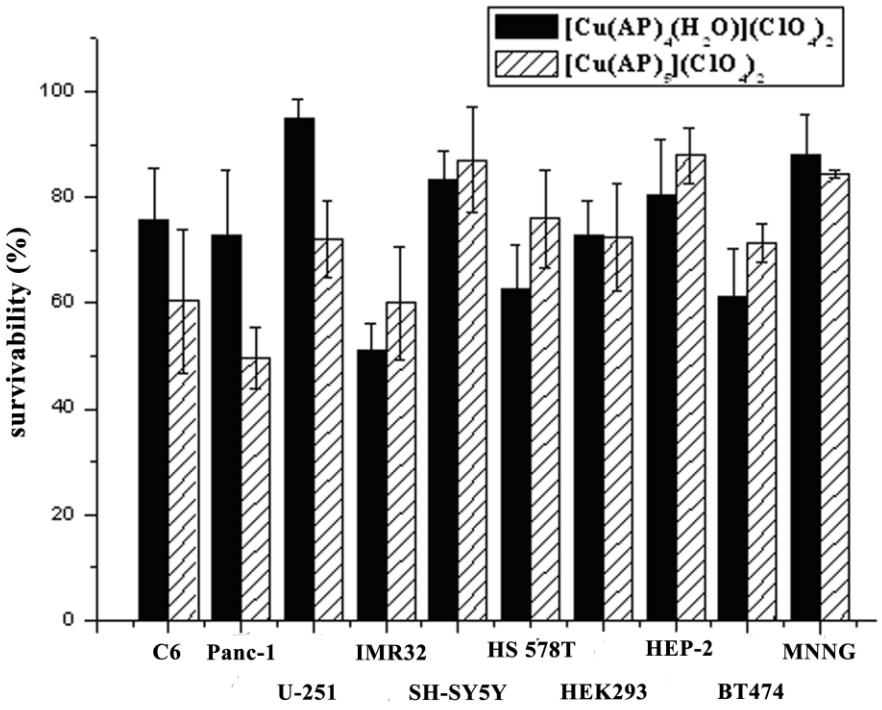

Figure S6. Sensitivity of different cell lines towards complex compounds (**1**) and (**2**) ($c = 1 \cdot 10^{-4}$ mol·dm^{-3}): C6 rat glioma, Panc-1 human pancreatic carcinoma. U-251 human glioma, IMR32 human neuroblastoma, HS 578-T and BT474 human breast cancer, HEK293 human embryonic kidney, Hep-2 Human Epithelioma-2, MNNG-HOS human osteosarcoma and SH-SY5Y human neuroblastoma-like cells.

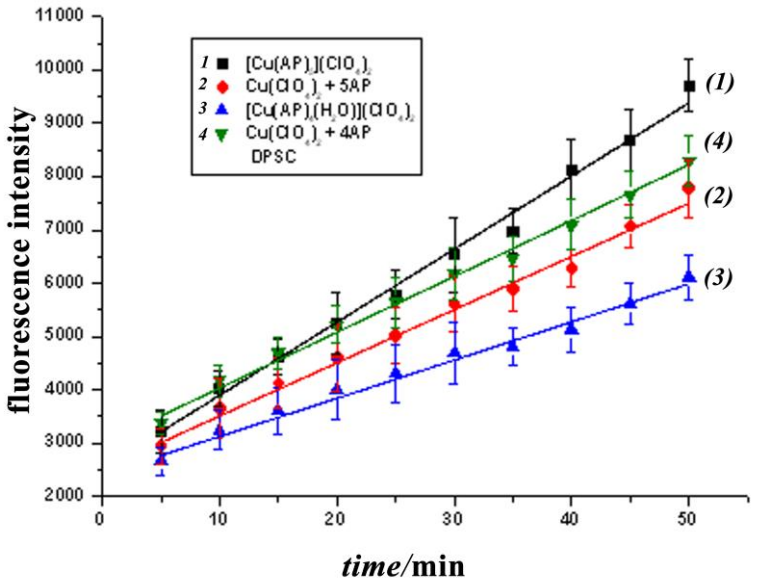

a)

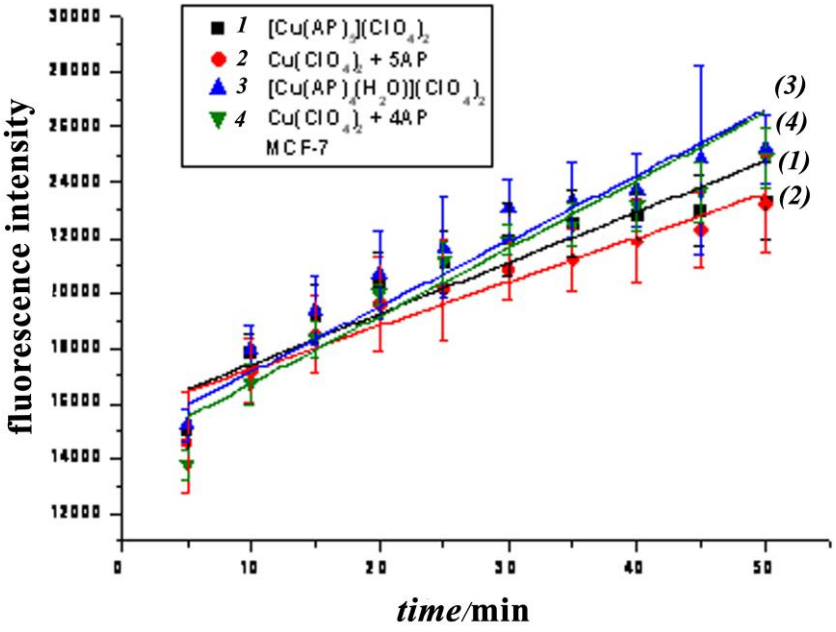

b)

Figure S7 Kinetics of ROS formation in the presence of complex compounds **1** and **2** or the respective stoichiometric mixtures ($c = 1 \cdot 10^{-4}$ mol·dm^{-3}); *a*) DPSC; *b*) MCF-7 cell line.

Dichlorofluorescin (DCFH) was used as a measure of reactive oxygen species.[48] The method is based on the fact that the nonpolar, nonionic 2',7'-dichlorofluorescin diacetate (DCFH-DA crosses cell membranes and is enzymatically hydrolyzed by intracellular esterases to nonfluorescent DCFH. In the presence of Reactive Oxygen Species (ROS), DCFH is rapidly oxidized to highly fluorescent 2',7'-dichlorofluorescein (DCF). DCFH-DA («MolecularProbes/Invitrogen», «CA», USA) was added to the cultured cells in 96-well plate template ($c = 5 \cdot 10^{-6}$ mol·dm^{-3}), then incubated for 30 min at 37° C and 5% CO_2. Then cells were washed with PBS-HEPES with subsequent addition of complex compound or the synergetic mixture of the initial compounds ($c = 1 \cdot 10^{-4}$ mol·dm^{-3}), Hydrogen peroxide ($c = 0.5 \cdot 10^{-3}$ mol·dm^{-3}) was used as a reaction progress indicator and cells cultured in DMEM/F12 – as a negative control. Cellular fluorescence was monitored on a Infinity 200 (Tecan, Austria) plate spectrofluorometer with excitation wavelength at 488 nm and emission wavelength 528 nm (Figure S7).

Table S1 IR-spectral data for $[Cu(AP)_4(H_2O)](ClO_4)_2$ **1** and $[Cu(AP)_5](ClO_4)_2$ **2**

$[Cu(AP)_4(H_2O)](ClO_4)_2$ (**1**)		$[Cu(AP)_5](ClO_4)_2$ **2**		AP	
Wavenumber cm^{-1}	Assignment	Wavenumber cm^{-1}	Assignment	Wavenumber cm^{-1}	Assignment
1602 w	δ(H-O-H)	1651 w	ν(C=O) weakly coordinated antipyrine	1666 VS	ν(C=O)
1574 VS	ν(Cu−O)+ν(C=O)	1566 VS	ν(Cu−O)+ν(C=O) strongly coordinated	1593 s	ν(CN + CC)
1496 s	ν(CN) + ν(CC)		antipyrine (1610 cm^{-1} [23])	1496 s	ν(CN + CC)
1380 w	δ(CH_3)	1488 s	ν(CN) + ν(CC)	1434 m	δ(CH_3)
1360 w	δ(CH_3)	1456 m	δ(CH_3)	1415 s	δ(CH_3)
1317 w	ρ(CH)(Ph) +pyrazolone ring deformation	1409 m	ν(CN) + δ(CH_3)	1375 m	ν(CN)+δ(CH_3)
		1367 w	δ(CH_3)	1325 s	ρ(CH)(Ph) + pyrazolone ring deformation
1299 w	ρ(CH)(Ph)+pyrazolone ring deformation	1309 w	ρ(CH)(Ph)+ pyrazolone ring deformation	1305 s	ρ(CH)(Ph)+ pyrazolone ring deformation
		1293 w	ρ(CH)(Ph)+pyrazolone ring deformation	1226 s	ρ(CH)(Ph)+pyrazolone ring deformation
1270 w	ρ(CH)(Ph)+pyrazolone ring deformation	1179 m	ρ(CH)(Ph)+pyrazolone ring deformation	1176 s	ρ(CH)(Ph)+pyrazolone ring deformation
		1145 s	ν(CC)+ +pyrazolone ring deformation	1136 s	ρ(CH)(Ph)+pyrazolone ring deformation
1182 m	ρ(CH)(Ph)+pyrazolone ring deformation	1082 VS	ν_3 (ClO_4)	1024 m	ρ(CH)(Ph)+pyrazolone ring deformation
		1006 w	ρ(CH)(Ph)+ δ(CH_3)	993 w	ρ(NCO)
1148 s	ν(CC) +pyrazolone ring deformation	988 w	ring breathing	817 m	χ(CCC)(Ph)
		808 w	χ(CCC)(Ph)	771 m	pyrazolone ring deformation
1101 VS	ν_3 (ClO_4)	769 s	χ(CCC)(Ph)+pyrazolone ring deformation	738 m	χ(CCC)(Ph) + pyrazolone ring deformation
1018 w	ρ(CH)(Ph)+ δ(CH_3)	724 s	ρ(CH)(Ph)+pyrazolone ring deformation		
985 w	ring breathing	694 s	ν_4 (ClO_4) + ρ(CH)(Ph) + pyrazolone ring	719 m	ρ(CH)(Ph) + pyrazolone ring deformation
870 m	χ(CCC)(Ph)		deformation	698 m	ρ(CH)(Ph) + pyrazolone ring deformation
792 w	χ(CCC)(Ph)+pyrazolone ring deformation	651 s	pyrazolone ring deformation		
		618 VS	ρ(CH)(Ph) + pyrazolone ring deformation		
763 s	pyrazolone ring deformation				
727 s	χ(CCC)(Ph)+pyrazolone ring deformation				
692 s	ν_4 (ClO_4)				

s-strong, m-medium, w-weak, VS- very strong

Table S2 Crystal data and structure refinement for compound $[Cu(AP)_4(H_2O)](ClO_4)_2$ (**1**)	
Compound	$[Cu(C_{11}H_{12}N_2O)_4(H_2O)](ClO_4)_2$
Empirical Formula	$C_{44}H_{50}Cl_2CuN_8O_{13}$
Formula weight	1033.36
Radiation, T, K	Mo Kα (λ = 0.71073), 150 K
Crystal system, Sp. gr., Z	Monoclinic, $P2_1/c$, 8
a, b, c, Å	27.4806(7), 25,2199(6), 13.7206(4)
α, β, γ, °; V, $Å^3$	90.00, 94.711(1), 90.00; 9477.0(4)
Crystal size, mm^3	0.50 x 0.35 x 0.18 Light-green, block
2Θ range for data collection, °	2.358-27.120
Index ranges	$-35 \leq h \leq 35$, $-32 \leq k \leq 32$, $-17 \leq l \leq 16$
Reflections collected /Independent reflections	150253/20903
Data/restraints/parameters	20903/0/1227
μ, mm^{-1}; ρ, $g \cdot cm^{-3}$	0.646 1.448
GOOF	1.016
R1/wR2 [I≥2σ(I)]; R1/wR2	0.0370/0.0839; 0.0511/0.0904
Largest diff. peak/hole/ e $Å^{-3}$	0.761/-0.808
Flack parameter	-

Table S3. Selected bond distances (Å) and angles (°) for $[Cu(C_{11}H_{12}N_2O)_4(H_2O)](ClO_4)_2$. (**1**)

Bond lengths					
Cu2–O1A	1.9205(12)	C12A–O2A	1.271(2)	C34A–N7A	1.379(2)
Cu2–O2A	1.9458(12)	C23A–O3A	1.260(2)	C1A–C2A	1.418(2)
Cu2–O3A	1.9385(12)	C34A–O4A	1.267(2)	C12A–C13A	1.414(2)
Cu2–O4A	1.9647(12)	C1A–N1A	1.365(2)	C23A–C24A	1.420(2)
Cu2–O5A	2.3003(12)	C12A–N3A	1.368(2)	C34A–C35A	1.409(2)
C1A–O1A	1.272(2)	C23A–N5A	1.383(2)		

Bond angles							
Atom	Atom	Atom	Angle	Atom	Atom	Atom	Angle
O1A	Cu2	O2A	89.45(5)	O2A	C12A	N3A	120.37(16)
O1A	Cu2	O3A	172.73(5)	O2A	C12A	C13A	133.59(17)
O1A	Cu2	O4A	89.08(5)	O3A	C23A	N5A	120.10(16)
O1A	Cu2	O5A	91.15(5)	O3A	C23A	C24A	133.59(17)
O2A	Cu2	O4A	154.63(5)	O4A	C34A	N7A	120.64(16)
O2A	Cu2	O5A	100.69(5)	O4A	C34A	C35A	133.07(17)
O3A	Cu2	O2A	90.96(5)	C1A	O1A	Cu2	124.84(11)
O3A	Cu2	O4A	87.44(5)	C12A	O2A	Cu2	126.64(12)
O3A	Cu2	O5A	95.91(5)	C23A	O3A	Cu2	132.38(12)
O4A	Cu2	O5A	104.66(5)	C34A	O4A	Cu2	125.81(11)
O1A	C1A	N1A	120.47(16)	N3A	C12A	C13A	106.04(15)
O1A	C1A	C2A	133.42(16)	N5A	C23A	C24A	106.30(15)
N1A	C1A	C2A	106.10(15)	N7A	C34A	C35A	106.29(15)

Table S4. Crystal data and structure refinement for compound $[Cu(AP)_5](ClO_4)_2$ (**2**)	
Compound	$[Cu(C_{11}H_{12}N_2O)_5](ClO_4)_2$
Empirical Formula	$C_{55}H_{60}Cl_2CuN_{10}O_{13}$
Formula weight	1207.57
Radiation, T, K	Mo Kα (λ = 0.71073), 100 K
Crystal system, Sp. gr., Z	Monoclinic, C 2/c, 8
a, b, c, Å	37.0018(11), 15.2340(5), 23.9586(7)
α, β, γ, °; V, $Å^3$	90.00, 122.8220(10), 90.00; 11349.1(6)
Crystal size, mm^3	0.18 x 0.14 x 0.12 green, block
2Θ range for data collection, °	3.98 - 52.8
Index ranges	$-46 \leq h \leq 46$, $-19 \leq k \leq 19$, $-29 \leq l \leq 29$
Reflections collected /Independent reflections	47097/11592
Data/restraints/parameters	11592/0/745
μ, mm^{-1}; ρ, $g \cdot cm^{-3}$	0.552, 1.413
GOOF	1.021
R1/wR2 [I≥2σ(I)]; R1/wR2	0.0442/0.1036; 0.0620/0.1124
Largest diff. peak/hole/ e $Å^{-3}$	0.66/-0.56
Flack parameter	-

Table S5. Selected bond distances (Å) and angles (°) for $[Cu(C_{11}H_{12}N_2O)_5](ClO_4)_2$ (**2**)

Bond lengths					
Cu1–O1	1.9552(18)	N1-C4	1.425(3)	N1D-C4D	1.434(3)
Cu1–O2	1.9379(15)	N1A–N2A	1.384(3)	N2-C3	1.366(3)
Cu1–O3	2.1699(16)	N1A–C1A	1.368(3)	N2-C10	1.463(3)
Cu1–O4	1.9923(17)	N1A–C4A	1.433(3)	N2A-C3A	1.344(3)
Cu1–O5	1.9559(15)	N1B–N2B	1.407(3)	N2A-C10A	1.457(3)
O1-C1	1.273(3)	N1B-C1B	1.388(3)	N2B-C3B	1.378(3)
O2-C1A	1.272(3)	N1B-C4B	1.428(3)	N2B-C10B	1.464(3)
O3-C1B	1.245(3)	N1C-N2C	1.398(3)	N2C-C3C	1.354(4)
O4-C1C	1.271(3)	N1C-C1C	1.381(3)	N2C-C10C	1.475(3)
O5–C1D	1.264(3)	N1C-C4C	1.420(3)	N2D-C3D	1.360(3)
N1–N2	1.395(3)	N1D-N2D	1.392(3)	N2D-C10D	1.464(3)
N1-C1	1.366(3)	N1D-C1D	1.376(3)		

Bond angles							
Atom	Atom	Atom	Angle	Atom	Atom	Atom	Angle
O1	Cu1	O3	111.21(8)	C1C	O4	Cu1	122.95(15)
O1	Cu1	O4	148.21(8)	C1D	O5	Cu1	117.88(14)
O1	Cu1	O5	89.52(7)	N2	N1	C4	121.00(19)
O2	Cu1	O1	89.59(7)	C1	N1	N2	109.5(2)
O2	Cu1	O3	94.56(7)	C1	N1	C4	126.7(2)
O2	Cu1	O4	90.15(7)	N2A	N1A	C4A	123.07(19)
O2	Cu1	O5	176.90(7)	C1A	N1A	N2A	108.5(2)
O4	Cu1	O3	100.50(7)	C1A	N1A	C4A	125.6(2)
O5	Cu1	O3	88.53(6)	N2B	N1B	C4B	119.09(18)
O5	Cu1	O4	89.05(7)	C1B	N1B	N2B	109.41(18)
C1	O1	Cu1	128.22(16)	C1B	N1B	C4B	126.8(2)
C1A	O2	Cu1	122.47(15)	N2C	N1C	C4C	120.1(2)
C1B	O3	Cu1	130.46(15)	C1C	N1C	N2C	108.5(2)

Table S6 Crystal data and structure refinement for compound $[Cu(CH_3CN)_4](ClO_4)$ (**3**)

Compound	$[Cu(CH_3CN)_4](ClO_4)$
Empirical Formula	$C_8H_{12}ClCuN_4O_4$
Formula weight	327.21
Radiation, T, K	Mo Kα (λ = 0.71073), 100 K
Crystal system, Sp. gr., Z	Orthorhombic, *P*an2$_1$, *Z* = 12
a, b, c, Å	23.8013(13), 8.3216(4), 20.3492(12)
α, β, γ, °; V, Å^3	90.00, 90.00, 90.00; 4030.5(4)
Crystal size, mm^3	0.18 x 0.14 x 0.08 Light yellow prism
2Θ range for data collection, °	2.634–28.268
Index ranges	$-30 \le h \le 31$, $-11 \le k \le 10$, $-27 \le l \le 27$
Reflections collected /Independent reflections	37652/9437
Data/restraints/parameters	9437/1/499
μ, mm^{-1}; ρ, g·cm^{-3}	1.836; 1.618
GOOF	1.066
R1/wR2 [I≥2σ(I)]; R1/wR2	0.0280/0.0651; 0.0303/0.0660
Largest diff. peak/hole/ e Å^{-3}	0.444/-0.421
Flack parameter	0.065(7)

Table S7. Selected bond distances (Å) and angles (°) for $[Cu(CH_2CN)_4](ClO_4)$ (**3**)							
Bond lengths							
Cu1–N1		1.996(2)	Cu2–N5		2.0004(18)	Cu3–N9	1.983(2)
Cu1–N2		1.972(2)	Cu2–N6		1.971(2)	Cu3–N10	1.9843(18)
Cu1–N3		2.009(2)	Cu2–N7		2.006(2)	Cu3–N11	1.974(2)
Cu1–N4		1.996(2)	Cu2–N8		2.005(2)	Cu3–N12	2.0017(18)
Bond angles							
Atom	Atom	Atom	Angle	Atom	Atom	Atom	Angle
N1	Cu1	N3	105.06(8)	N6	Cu2	N7	112.47(9)
N2	Cu1	N1	110.82(9)	N6	Cu2	N8	110.56(9)
N2	Cu1	N3	108.52(9)	N8	Cu2	N7	105.46(8)
N2	Cu1	N4	112.90(9)	N9	Cu3	N10	109.41(9)
N4	Cu1	N1	110.60(8)	N9	Cu3	N12	107.87(9)
N4	Cu1	N3	108.60(8)	N10	Cu3	N12	107.66(7)
N5	Cu2	N7	106.57(8)	N11	Cu3	N9	111.04(8)
N5	Cu2	N8	109.94(8)	N11	Cu3	N10	111.98(9)
N6	Cu2	N5	111.60(8)	N11	Cu3	N12	108.73(9)

Table S8. Bond lengths (Å), Δ_rG_{298}, Δ_rG_{298}(PCM) kcal·mol^{-1}

Composition	R (Cu-O), Å. exp.	R (Cu-O), Å, calc.	reaction	Δ_rG_{298}, kcal·mol^{-1}	Δ_rG_{298}(PCM), kcal·mol^{-1}
1	2	3	4	5	6
$[Cu(AP)_4(H_2O)]^{2+}$	1.9488(12), 1.9389(12), 1.9467(12), 1.9445(12), 2.2630(13) (water)	2.015, 1.992, 1.969, 1.973, 2.535 (water)	$[Cu(H_2O)_4]^{2+}$ + 4AP = $[Cu(AP)_4(H_2O)]^{2+}$ + $3H_2O$	-157.96	**-21.94**
$[Cu(AP)_5]^{2+}$	1.9552(18), 1.9379(15) 2.1699(16) 1.9923(17) 1.9959(15	2.266, 2.021, 2.007, 2.000, 2.000	$[Cu(H_2O)_4]^{2+}$ + 5AP = $[Cu(AP)_5]^{2+}$ + $4H_2O$	-162.80	**-12.89**
$[Cu(AP)_4]^{2+}$	–	1.957, 1.969, 1.970, 1.964	$[Cu(H_2O)_4]^{2+}$ + 4AP = $[Cu(AP)_4]^{2+}$ + $4H_2O$	-160.67	**-29.46**
$[Cu(AP)_5]^{2+}$*AP	–	2.011, 1.995, 2.003, 2.007, 2.297(ax), 4.425(ax)	$[Cu(H_2O)_4]^{2+}$ + 6AP = $[Cu(AP)_5]^{2+}$*AP + $4H_2O$	-161.55	**5.44**
$[Cu(AP)_4(CH_3CN)]^{2+}$		2.002, 2.001, 1.989, 2.010, 2.345 (Cu-N)	$[Cu(H_2O)_4]^{2+}$ + 4AP + CH_3CN = $[Cu(AP)_4(CH_3CN)]^{2+}$ + $4H_2O$	-159.04	**-20.36**

Table S9. Cytotoxic effect of complex compounds and stoichiometric mixtures on DPSC (survivability, % to control)				
Compound or mixture	Concentration, $mol \cdot L^{-1}$			
	$1 \cdot 10^{-5}$	$5 \cdot 10^{-5}$	$1 \cdot 10^{-4}$	$5 \cdot 10^{-4}$
$[Cu(AP)_4(H_2O)](ClO_4)_2$ (**1**)	93,72±2,70	68,36±5,89	51,50±9,40	12,83±5,46
$Cu(ClO_4)_2$+4AP	97,49±7,16	86,2±4,43	56,12±6,10	34,65±2,52
$[Cu(AP)_5](ClO_4)_2$ (**2**)	100,69±6,50	99,46±10,18	75,36±11,08	17,75±4,31
$Cu(ClO_4)_2$+5AP	98,53±3,23	94,02±8,12	80,86±12,96	64,93±13,36
$Cu(ClO_4)_2$	68,36±7,91	48,45±10,27	43,57±8,11	-
AP	98,75±13,96	85,12±9,032	65,32±9,15	-
Dox (doxorubicin)	79,09±5,63	64,87±12,68	58,79±10,92	-

Table S10. Cytotoxic effect of complex compounds and stoichiometric mixtures on MCF-7 cell line (survivability, % to control)				
Compound or mixture	Concentration, $mol \cdot L^{-1}$			
	$1 \cdot 10^{-5}$	$5 \cdot 10^{-5}$	$1 \cdot 10^{-4}$	$5 \cdot 10^{-4}$
$[Cu(AP)_4(H_2O)](ClO_4)_2$ (**1**)	94,08±5,28	60,72±5,66	56,54±8,44	28,99±3,41
$Cu(ClO_4)_2$+4AP	95,41±4,30	78,42±17,89	47,23±6,10	38,73±8,31
$[Cu(AP)_5](ClO_4)_2$ (**2**)	97,79±7,64	77,23±7,35	58,345±9,94	47,55±13,08
$Cu(ClO_4)_2$+5AP	100,05±4,01	96,71±11,29	83,88±11,59	68,35±4,72
$Cu(ClO_4)_2$	91,34±10,47	81,46±6,58	72,61±6,72	-
AP	99,97±14,23	106,4±9,90	104,06±13,02	-
Dox (doxorubicin)	81,73±9,23	68,97±7,55	39,76±5,09	-